

In Vitro Culture and Directed Osteogenic Differentiation of Human Pluripotent Stem Cells on Peptides-Decorated Two-Dimensional Microenvironment

Mengke Wang,^{†,‡} Yi Deng,^{†,§} Ping Zhou,^{†,§} Zuyuan Luo,^{†,§} Qihong Li,^{§,||} Bingwu Xie,^{§,⊥} Xiaohong Zhang,^{†,§} Tong Chen,[‡] Duanqing Pei,^{||} Zhihui Tang,^{*,‡} and Shicheng Wei^{*,†,‡,§}

[†]Department of Oral and Maxillofacial Surgery, Laboratory of Interdisciplinary Studies, School and Hospital of Stomatology, Peking University, Beijing 100081, People's Republic of China

[‡]Second Dental Center, School and Hospital of Stomatology, Peking University, No. 66 An-Li Road, Chao-Yang District, Beijing 100081, People's Republic of China

[§]Center for Biomedical Materials and Tissue Engineering, Academy for Advanced Interdisciplinary Studies, Peking University, Beijing 100871, People's Republic of China

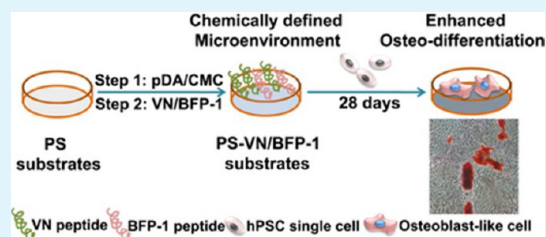
^{||}Key Laboratory of Regenerative Biology, Guangzhou Institutes of Biomedicine and Health, Chinese Academy of Sciences, Guangzhou, 510530, People's Republic of China

[⊥]Chongqing Key laboratory for Oral Diseases and Biomedical Sciences, Chongqing Medical University, Chongqing 400015, People's Republic of China

Supporting Information

ABSTRACT: Human pluripotent stem cells (hPSCs) are a promising cell source with pluripotency and capacity to differentiate into all human somatic cell types. Designing simple and safe biomaterials with an innate ability to induce osteoblastic lineage from hPSCs is desirable to realize their clinical adoption in bone regenerative medicine. To address this issue, here we developed a fully defined synthetic peptides-decorated two-dimensional (2D) microenvironment via polydopamine (pDA) chemistry and subsequent carboxymethyl chitosan (CMC) grafting to enhance the culture and osteogenic potential of hPSCs in vitro. The hPSCs including human embryonic stem cells (hESCs) and human induced pluripotent stem cells (hiPSCs) were successfully cultured on the peptides-decorated surface without Matrigel and ECM protein coating and underwent promoted osteogenic differentiation in vitro, determined from the alkaline phosphatase (ALP) activity, gene expression, and protein production as well as calcium deposit amount. It was found that directed osteogenic differentiation of hPSCs was achieved through a peptides-decorated niche. This chemically defined and safe 2D microenvironment, which facilitates proliferation and osteo-differentiation of hPSCs, not only helps to accelerate the translational perspectives of hPSCs but also provides tissue-specific functions such as directing stem cell differentiation commitment, having great potential in bone tissue engineering and opening new avenues for bone regenerative medicine.

KEYWORDS: human pluripotent stem cells, osteogenic differentiation, carboxymethyl chitosan, peptide, polydopamine



1. INTRODUCTION

Bone defects resulting from trauma, osteoporosis, congenital malformations, and surgical resections remain a serious fast-growing challenge in the medical area worldwide, and the associated annual healthcare expenditures are estimated to be tens of billions of dollars with a significant increase for the next decades.^{1,2} Current treatments of large bone defects, which rely on the use of autologous grafts (the “gold standard” of bone substitution) and transplantation of allograft, have limited clinical potential due to their inherent limitations, such as donor site morbidity, available quantities, and host immune rejection.³ Therefore, innovative bone tissue engineering approaches are required to develop effective therapies for complex bone reconstructions.

One of the alternative valid therapies involves the combination of scaffolds with a source of osteogenic cells. It is widely believed that the use of stem cells induces greater bone regeneration than transplanting bone substitute materials alone into bone defects.^{4–6} Several types of human mesenchymal stem cells (hMSCs), such as human bone mesenchymal stem cells (hBMSCs)^{7,8} and human adipose-derived stem cells (hADSCs),^{4,9} have been highlighted previously as selectable cell sources for bone regeneration purposes, and some prospective results have been achieved. For

Received: October 20, 2014

Accepted: February 11, 2015

Published: February 11, 2015

instance, biomimetic tissue-engineering strategies have been explored for the ex vivo cultivation of analogous bone substitutes via culturing and osteo-differentiating hMSCs.¹⁰ hMSCs, however, have to be isolated from bony tissue biopsy, and surgical bone marrow aspirations yield very limited numbers of hMSCs.¹¹ Moreover, the low proliferation rate of adult hMSCs limits their expandability under culture conditions and their capacity to differentiate into new osteoblasts decreases with aging.^{12,13} These imperfections hinder hMSCs to be an excellent option for bone-repairing treatments in clinic.

Human pluripotent stem cells (hPSCs), which include both human embryonic stem cells (hESCs) and human induced pluripotent stem cells (hiPSCs), have the potential to give rise to all major lineages of somatic cells and therefore have become promising candidates for regenerative medicine.^{14–16} Compared with hESCs, hiPSCs developed from human autologous somatic cells could circumvent concerns regarding immune properties and ethical issues, making them an ideal cell source for regenerative medicine.¹⁷ In terms of bone regenerative therapies, despite of the advantages that hPSCs offer, controlling their differentiation into bone-functional cells remains a tough challenge. In addition, the safety of these cell products has already drawn broad attention, even though the clinical application of hPSCs is still at its infant stage. To date, Matrigel-coated and extracellular matrix (ECM) protein-immobilized (such as vitronectin, fibronectin, and laminin) surface are the most popular substrates for hPSCs culture and differentiation based on the literature and reports.^{18–21} Matrigel is an extraction from Englebreth–Holm–Swarm (EHS) mouse sarcomas containing not only basement membrane components but also numerous growth factors, inhibitors, and a broad variety of unknown proteins. The significant quality variance of Matrigel and isolated ECM proteins from lot-to-lot confounds basic research to dissect the molecular mechanisms.²² Additionally, the presence of animal or human proteins causes problems related to immunogenicity and microbial and viral contamination and eventually limits their applications in clinic.^{23,24} Thus, successful integration of hPSCs into clinical bone regenerative applications will require chemically defined and safe conditions for expansion of hPSCs followed by regulating their lineage commitment to osteoblasts.

Synthetic peptides have been widely used for the proliferation and osteogenesis of a variety of cell types.^{25,26} For culturing and differentiating hPSCs, the peptides derived from ECM proteins could offer significant advantages, because they are generated from defined chemical structures and processes, and there is no variation between batches. More importantly, eliminating the need for animal/human by-products eradicates concerns regarding immunogenicity and shows greater potential for clinic. Recently, a synthetic RGD oligopeptide derived from vitronectin (VN) was reported to support the adhesion and successful self-renewal of hESCs and hiPSCs for >15 passages.^{27,28} On the other hand, a new bone-forming peptide BFP-1 [GQGFSYPYKAVFSTQ sequence] from bone morphogenetic protein-7 (BMP-7) demonstrated by Kim et al. had more osteogenic activity than BMP-7 and induced osteogenesis of hMSCs.^{29,30} Despite progress in the development of novel matrices for expansion of hPSCs, a peptides-decorated cell niche enabling hPSCs to proliferate and directed osteogenic differentiate under fully defined conditions for bone regenerative medicine, to our best knowledge, has yet to be explored, and there are barely any reports regarding the impact of BFP-1 peptide on osteogenesis of hPSCs. In this

study, a VN/BFP-1 mixed peptides-modified 2D polystyrene (PS) cell culture plate was established for enhancing the culture and osteogenic potential of hPSCs in vitro assisted by polydopamine (pDA) technology. Carboxymethyl chitosan (CMC), a water-soluble chitosan derivative, is a natural linear amino-polysaccharide with a large number of amine and carboxyl groups. With excellent biocompatibility, biodegradability, nonimmunogenicity, and intrinsic antibacterial properties, CMC finds a wide range of applications in medicine.^{31–33} Meanwhile, it is also reported that CMC, a structure similar to glycosaminoglycans, can induce osteogenic differentiation of cells.^{34,35} In order to better immobilize the peptide onto the pDA-coated substrate, CMC as a bridge was grafted to pDA coating through the abundant primary amines of CMC reacting with the oxidized catechol groups for a large amount of peptide tethering.³¹ We believe that VN peptide could facilitate the adhesion and proliferation of hPSCs, and the osteoinductive peptide derived from BMP-7 could enhance the differentiation of hPSCs into the osteogenic lineage. A further comprehensive in vivo evaluation on bone formation of the differentiated osteogenic precursors generated from the peptides-decorated substrate is currently underway in the laboratory. The completely synthetic peptide substrate developed for hPSCs culture/osteo-differentiation has achieved consistent osteogenesis of hPSCs in chemically defined conditions in vitro and will greatly accelerate the introduction of hPSCs into bone-repairing clinical applications.

2. MATERIALS AND METHODS

2.1. Materials. Dopamine hydrochloride (DA) was purchased from Sigma-Aldrich (St. Louis, USA), and Tris[hydroxymethyl]animomethane (Tris-HCl) was provided by Sinopharm Chemical Reagent Co. Ltd. (Beijing, China). *N*-(3-(Dimethylamino)propyl)-*N'*-ethylcarbodiimide hydrochloride (EDC), *N*-hydroxysuccinimide (NHS), 2-(*N*-morpho)ethanesulfonic acid (MES), carboxymethyl chitosan (CMC), and phosphate buffer (PBS) were obtained from Aladdin (Shanghai, China). To facilitate chemical conjugation onto the material surface, the peptide was modified at its *N*-terminal with a lysine-containing spacer. VN peptide [Ac-KGGPQVTRGDVFTMP sequence] and BFP-1 peptide [Ac-KGGQGFSYPYKAVFSTQ sequence], provided by Chinapeptides Co. Ltd. (Shanghai, China), were synthesized by a batchwise fmoc-poly-amide method and had more than 98% purity per the high-pressure liquid chromatography profile. All other chemicals were of analytical reagent grade, and all aqueous solutions were prepared with deionized water (D.I. water).

2.2. Preparation of the Carboxymethyl Chitosan-Coated Surface via Polydopamine. The 6-well PS cell culture plates (Corning, USA) were first immersed into a dopamine solution (2 mg/mL in 10 mM Tris-HCl, pH = 8.5) with shaking for 24 h at ambient temperature. The pDA-modified PS surfaces were then rinsed with D.I. water to remove the unattached dopamine (denoted as PS-pDA). Afterward, the CMC macromolecular was grafted onto the PS-pDA by immersing the substrates in 5 mL/well of 3 w/v % CMC solution for another 24 h at 37 °C in a constant temperature shaker. The treated substrates were then washed with D.I. water to remove the physically adsorbed CMC molecular, which were named as PS-CMC.

2.3. Immobilization of VN and BFP-1 Peptide. VN and BFP-1 peptide were dissolved in sterilized PBS with a concentration of 1 mM, separately, and then the different peptide combinations were mixed in various volume ratios (VN:BFP-1 = 10:0, 7:3, and 5:5). To immobilize VN and BFP-1 peptide on the surface, the PS-CMC samples were pretreated by 2 mM EDC and 5 mM NHS in 0.1 M MES buffer (pH = 5.6) for 40 min in superclean bench. Then, various peptides combination solutions were incubated on the carboxyl-rich PS-CMC surfaces in a 4 °C refrigerator for 24 h. The final decorated PS substrates were thoroughly washed by D.I. water and dried under nitrogen influx before characterization and cell experiment. Peptides-

conjugated PS substrates prepared from different volume ratios of VN/BFP-1 were named PS-VN₁₀, PS-VN₇/BFP₃, and PS-VN₅/BFP₅.

2.4. Surface Characterization. PS with and without pDA/CMC/peptide modifications were characterized by contact angle goniometry, X-ray photoelectron spectroscopy (XPS), and scanning electron microscope (SEM), as well as atomic force microscopy (AFM). The surface hydrophilicity was measured by contact angle goniometry with a Dataphysics OCA20 contact angle system (Filderstadt, Germany) at ambient temperature based on the sessile drop method. Six parallel specimens were used to provide an average and standard deviation. The alteration of chemical composition was analyzed by X-ray photoelectron spectroscopy (XPS, Kratos Analytical Ltd., UK) for both survey and high-resolution spectra. The binding energies were calibrated by the C 1s hydrocarbon peak at ~285 eV; besides, the quantitative analysis and curve fitting were conducted using the CasaXPS software package. In addition, the surface morphologies of the treated substrates were characterized by a field emission scanning electron microscope (FE-SEM, JSM-6701F, Japan) at an accelerating voltage of 20 kV. All samples were coated by gold for 1 min before SEM observation. AFM measurement and quantitative mechanical characterization were performed using a Bruker MultiMode 8 scanning probe microscope (Veeco, USA), operated under peak-force tapping mode with 1.0 Hz scan rates and a 200 mV amplitude set point. The silicon tip (spring constant 40 N m⁻¹, frequency 300 kHz, RTEP, USA) was irradiated with UV light to remove any organic contaminants before use. To calculate the Young's modulus, the retract curve of the force versus separation plots was fitted by the Derjaguin–Muller–Toporov (DMT) model.

2.5. Quantification of Peptide Content by Fluorescent Labeling. To quantify the peptide immobilized at different volume ratios, the FITC-labeled VN peptide and Rhodamine-labeled BFP-1 peptide were anchored on the PS-CMC surfaces to obtain a standard calibration curve of fluorescence intensity. Briefly, a dilution series of FITC-labeled VN peptide and Rhodamine-labeled BFP-1 peptide solution (varying from 0 to 1.2 mM) in acetonitrile:water (50:50) mixture was prepared. A 100 μ L amount of solution was dried down into wells of a 24-well plate coated with CMC (as described in section 2.2, PS-CMC preparation). The fluorescence intensity was determined using a Multilabel Reader (2300, Perkin Elmer, Singapore) at 488 nm excitation wavelength and 525 nm emission wavelength for FITC and at 532 nm excitation wavelength and 582 nm emission wavelength for Rhodamine. The peptide density was estimated by averaging the amount of the dried down peptide over the microwell surface area (1.9 cm²). Six independent measurements were performed for each condition.

The qualitative intensity and distribution of fluorescence of peptide-decorated surface were detected by inverted fluorescent microscopy (Nikon Eclipse TE2000-U, Japan). Furthermore, the quantitative average fluorescence intensity of the mixed-peptides modified surfaces was also determined using a Multilabel Reader. Six independent measurements were performed for each surface.

2.6. Cell Culture. The hiPSCs (UMC1-C1 line, provided by GIBH, Chinese Academy of Sciences, Guangzhou, China) were generated from umbilical cord mesenchymal cells by retroviral introduction of four Yamanaka's factors: Oct3/4, Sox2, Klf4, and c-Myc. The hESCs (H9 line, supplied from GIBH, Chinese Academy of Sciences) from the inner cell mass (ICM) of blastocyst-stage embryos were also used in the present study. Two sorts of hPSCs were cultured on Matrigel-coated plates using chemically defined mTeSR1 medium (StemCell Technologies, Canada) at 37 °C in a humidified 5% (v/v) CO₂ incubator (MCO-18AIC, Japan). Matrigel (BD Biosciences, Canada) was diluted with Dulbecco's modified eagle medium/F12 (DMEM/F12, Gibco, USA) at a ratio of 1:80 at 4 °C. Cells were fed daily and passaged at a 1:3 splitting ratio every 3–4 days by exposure to Dispase (Invitrogen, Canada) at 0.5 mg/mL for 5.5 min.

2.7. Osteogenic Differentiation. All samples were sanitized with 75% ethanol for at least 40 min before cell culture. hPSCs were dissociated to single cells via Accutase (StemCell Technologies) and then reseeded to tissue culture plastic, the pure CMC-modified substrate (PS-CMC), and the various peptides-decorated substrates

(PS-VN₁₀, PS-VN₇/BFP₃, and PS-VN₅/BFP₅ group) at a density of 1.6×10^5 cells/mL. The single cells were attached to the substrates in mTeSR1 medium for 1 day. An inverted phase contrast microscope (Nikon Eclipse TE2000-U) was used to image the cell adhesion and morphology on these surfaces. After cell adhesion, the culture medium was replaced by osteogenic inducing medium (OM) consisting of α -minimal essential medium (α -MEM, Invitrogen) supplemented with 10^{-8} M dexamethasone (DEX, Sigma-Aldrich), 5 μ g/mL ascorbic acid (AA, Sigma-Aldrich), and 10 mM β -glycerophosphate (β -GP, Sigma-Aldrich) combined with 100 μ g/mL streptomycin (Amresco, USA) and 100 U/mL penicillin (Amresco). In order to compare the osteogenic outcome, hMSCs treated with BMP-7 (1 μ g/mL in OM medium) was served as positive control, and hPSCs seeded on tissue culture plastic was used as negative control. Besides, hPSCs cultured with mTeSR1 medium (PM) on bare VN peptide-decorated substrate (i.e., PS-VN₁₀) was also used as control. The culture medium was changed every 2 days, and the whole process lasted for 28 days. Day 1 was referred to the day when osteogenic induction commenced.

2.8. Immunofluorescence. The hPSCs before osteoinductive differentiation (denoted as day 0) on pure VN peptide-decorated surface were subjected to immunofluorescence analysis. They were fixed with 4% (v/v) paraformaldehyde for 15 min and permeabilized with 0.1% (v/v) Triton X-100 (Solarbio, Beijing, China) for 30 min at room temperature. Afterward, they were incubated with 3% bovine serum albumin/PBS buffer at 37 °C for 2 h to block nonspecific binding. Cells were incubated with diluent primary antibodies against human Oct-4 (1:500, Cell Signaling Technology, USA) and Runx-2 (1:3200, Cell Signaling Technology) overnight at 4 °C. The next day, cells were incubated with secondary antibody at a dilution of 1:1000 for 1 h in the dark at ambient temperature (Goat Anti-Mouse 488 IgG, Goat Anti-Rabbit 543 IgG, Cell Signaling Technology). Finally, cell nuclei were stained with DAPI (10 μ g/mL, Sigma-Aldrich) for 5 min at room temperature. All staining steps were followed by three washes in PBS buffer. The stained signals in the cells were visualized immediately by laser confocal microscopy (LSM5, Carl Zeiss, Germany).

2.9. Cell Viability Assay. Cell viability of hiPSCs and hESCs was assessed by the cell counting kit-8 assay (CCK-8, Dojindo, Japan). After cell counting, the single cells were seeded on these peptides-decorated substrates at a density of 1.6×10^5 cells/mL. At desired time intervals (days 1, 3, 5, and 7) of cultivation, CCK-8 solution was added into each well at a proportion of 1:10 (v/v) for 2 h incubation in the dark. Then 100 μ L of supernatant from each well was transferred to new 96-well cell culture plates. The absorbance value of the supernatant optical density (OD value) for each group was measured with a microplate reader (model 680, Bio-Rad, Canada) at 450 nm. Six parallel specimens were used to provide an average and standard deviation.

2.10. Integrin-Blocking Assay. Integrin-blocking assay was carried out as described previously with some modifications.^{21,28} Briefly, hESCs and hiPSCs were dissociated to single cells, counted, and incubated for 30 min at 37 °C in the presence or absence of 10 μ g/mL human integrin $\alpha_v\beta_3$ antibodies (R&D systems, USA) in phenol red-free Iscove's modified Dulbecco's medium (IMDM) (Invitrogen) containing 0.35% (w/v) bovine serum albumin (BSA, Sigma-Aldrich). After incubation, cells were collected by centrifugation at 1200 rpm for 5 min and then resuspended in mTeSR1 medium, followed by seeding onto VN peptide-decorated 6-well plates at a density of 1.6×10^5 cells/mL and culturing at 37 °C for 1 h. Nonattached cells were carefully removed by washing the wells three times with IMDM/0.35% BSA and finally once with PBS. The attached cells were fixed with 100% ethanol at room temperature for 5 min and stained with 0.4% (w/v) crystal violet in methanol for 5 min at room temperature, followed by a thorough wash with D.I. water. Cell attachment was visually scored by a scanner (ScanMaker i800, MICROTOK, Shanghai, China) and quantified by CCK-8 assay.

2.11. Alkaline Phosphate (ALP) Activity Staining and Quantification. For ALP staining, the hPSCs on pure VN peptide-decorated surface were first fixed by 95% cold ethanol for 30 min, followed by three washes in PBS buffer. Afterward, the staining was

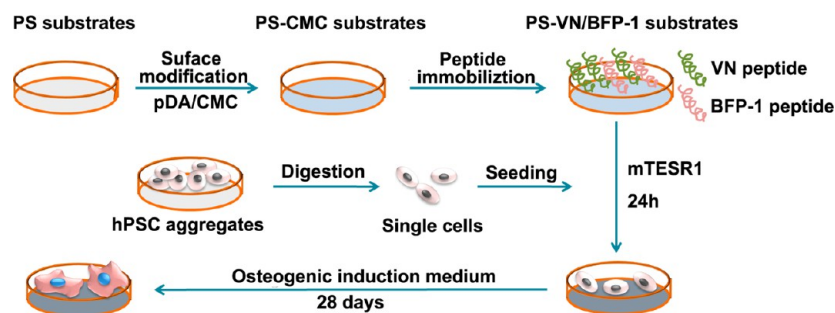


Figure 1. Schematic illustration of the preparation of peptides-decorated microenvironment and the in vitro directed osteogenic differentiation of the hPSCs (including hiPSCs and hESCs).

performed using an ALP detection kit (CW-BIO, Beijing, China) for 15 min per the product's instructions. Then the cells were observed under a phase contrast microscope (Nikon Eclipse TE2000-U) using white light. Quantification of ALP activity of hPSCs was carried out by an assay reagent kit (NJJC-BIO, Nanjing, China). Briefly, after 0, 4, 7, 14, and 21 days of cultivation, the cell layers were washed with frozen PBS and scraped off from the surfaces using 200 μL of 1% TritonX-100 (lysis solution) per well. After sonication and centrifugation at 12 000 rcf for 30 min, 30 μL of cell lysates at each well was transferred to new 96-well cell culture plates and cultivated with 50 μL of carbonated buffer solution (pH = 10) and 50 μL of substrate solution (4-amino-antipyrine) at 37 $^{\circ}\text{C}$ for 15 min. Then 150 μL of potassium ferricyanide was added into the above solution, and the production of *p*-nitrophenol was determined by the absorbance at 405 nm. For normalization, the total protein concentration was determined by Pierce BCA protein assay kits (Thermo, USA) with BSA as a standard. Finally, ALP activity was normalized and expressed as the total protein content (U/g of prot).

2.12. Alizarin Red S Staining. Mineralized nodule formation was determined on day 28 of osteoinductive differentiation by staining with Alizarin Red S (ARS) solution (Sigma-Aldrich). ARS was dissolved in D.I. water at a concentration of 2% (w/v) and adjusted to pH = 4.2. The cells on the substrates were washed with frozen PBS buffer and fixed in 4% formalin for 30 min. The fixed cells were further washed with D.I. water in order to remove any salt residues, and then ARS solution was added so that it covered the entire surface of the wells containing cells. After 20 min incubation at room temperature, the excess ARS was fully washed with D.I. water. The calcium deposited on the substrates in each group was observed under the inverted phase contrast microscope (Nikon Eclipse TE2000-U). To quantify the orange-red coloration of ARS, the substrates were immersed in hexadecylpyridinium chloride (1 w/v%, Sigma-Aldrich) overnight with shaking to dissolve the calcium mineral deposited by the cells. The 100 μL of supernatants was collected to new 96-well cell culture plates, and OD₄₉₀ was read using a microplate reader (model 680, Bio-Rad).

2.13. Quantitative Real-Time Polymerase Chain Reaction (qPCR). The total mRNA was isolated from cells using TRIzol (Invitrogen) and converted into cDNA using a Revert Aid First Strand cDNA Synthesis Kit (Thermo). Quantitative real-time polymerase chain reaction (qPCR) analysis was carried out with SYBR Green (Roche, USA) on an ABI 7500 RT-PCR machine (Applied Biosystems, USA). All items were performed in triplicate, and glyceraldehyde 3-phosphate dehydrogenase (GAPDH) was used as an internal control for PCR amplification. Primers (5'-3') provided in this study are listed in Table S1, Supporting Information. Primer sets (10 μM final concentration for each primer) were used in a volume of 20 μL per tube. The thermal profile of the PCR was 50 $^{\circ}\text{C}$ for 2 min, 95 $^{\circ}\text{C}$ for 10 min, followed by 40 cycles at 95 $^{\circ}\text{C}$ for 15 s and 60 $^{\circ}\text{C}$ for 1 min. The comparative CT ($2^{-\Delta\Delta\text{CT}}$) method was employed to evaluate fold gene expression differences between groups.

2.14. Western Blotting. Cells were harvested, flushed three times with ice-cold PBS, and lysed in RIPA buffer (HXBC-BIO, Beijing, China) containing protease inhibitor cocktail (HXBC-BIO) for 30 min

in ice. After centrifugation at 12 000 rcf for 30 min, 1 μL of supernatant was collected to determine the protein concentration using Pierce BCA protein assay kits (Thermo). An equal amount (15 μg) of protein was separated on 10% sodium dodecyl sulfate polyacrylamide gel electrophoresis (SDS-PAGE) gel and transferred to a nitrocellulose membrane. Membrane-transferred proteins were incubated in 5% nonfat milk for at least 1 h to block nonspecific binding. Afterward, membranes were probed with primary antibodies against human Oct-4 (1:1000, Cell Signaling Technology), Runx2 (1:900, Cell Signaling Technology), and GAPDH (1:1000, ZSGB-BIO, Beijing, China) at 4 $^{\circ}\text{C}$ overnight, followed by a corresponding horseradish peroxidase (HRP)-conjugated second antibodies (1:10 000, anti-rabbit/mouse IgG, ZSGB-BIO) for 1 h at room temperature. All staining steps were followed by three washes in Tris-buffered saline with tween (TBST) buffer. Finally, the membranes were detected by enhanced chemiluminescence on a Fusion Fx5 system (Vilber Lourmat, French).

2.15. Statistical Analysis. All data were expressed as mean \pm standard deviations. One-way analysis of variance (ANOVA) Tukey post-hoc test was used to determine the significant differences among the groups, and *p* values less than 0.05 were considered statistically significant.

3. RESULTS AND DISCUSSION

3.1. Preparation and Characterization of Peptides-Decorated Microenvironment. In this study, pDA-mediated catechol functionalization was applied to develop a 2D peptides-decorated microenvironment with greater osteoinductivity that can boost the osteogenic potential of hPSCs in vitro (Figure 1). Dopamine, a repeated motif in mussel adhesive protein, could undergo self-polymerization and adhere onto almost any solid surface in alkaline solution without surface pretreatments. More importantly, a pDA layer can function as an anchor to graft the secondary functional biopolymers by thiols and amines via Michael addition or Schiff base reactions.^{36–39} To better immobilize peptide on the surface of a PS culture plate presenting pDA coating, CMC molecule was further grafted to the pDA layer through the catechol chemistry, of which the amines of CMC could react with the oxidized catechol groups. The $-\text{COOH}$ groups on the resulting PS-CMC surfaces were preactivated with the EDC/NHS approach to facilitate the peptide tethering of terminal carboxyl groups to the NHS groups, producing peptide tethering surfaces.

To explore the alterations of chemical composition and morphology after various stages of surface functionalization, the prepared peptides-decorated microenvironment was characterized by contact angle goniometry, XPS, and SEM, as well as AFM analysis. There were no detectable differences in the chemical component and surface topography between PS-VN₁₀, PS-VN₇/BFP₃, and PS-VN₅/BFP₅ samples; therefore, PS-VN₅/

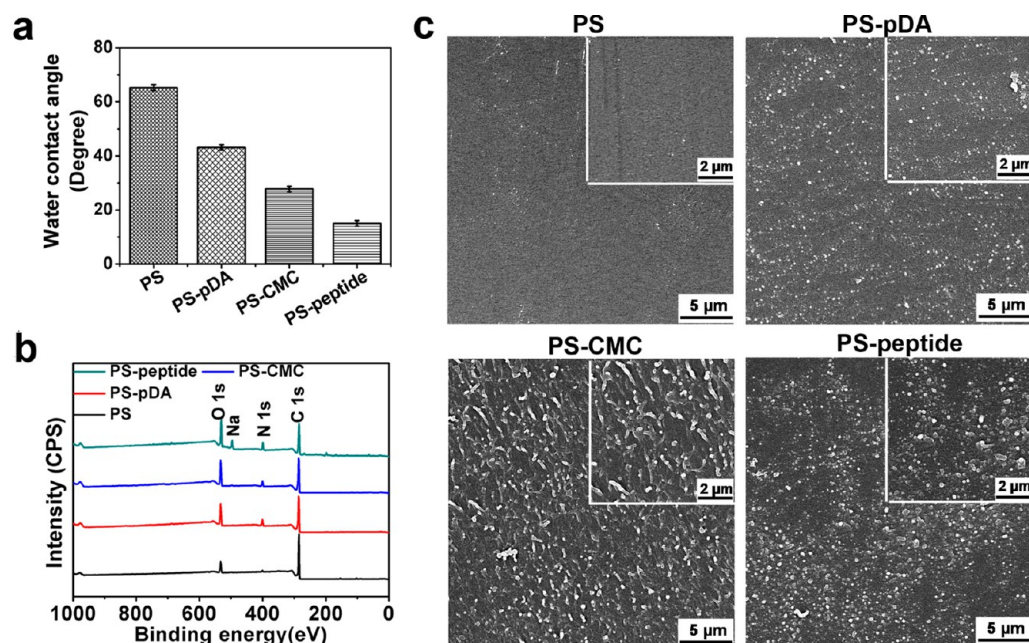


Figure 2. Surface characterization of the pristine and functionalized PS substrates (PS-pDA, PS-CMC, and PS-peptide). (a) Water contact angles. Data are displayed as mean \pm standard errors ($n = 6$). (b) XPS survey scan spectra. (c) SEM morphology with low (scale bar $5 \mu\text{m}$) and high (scale bar $2 \mu\text{m}$) magnification.

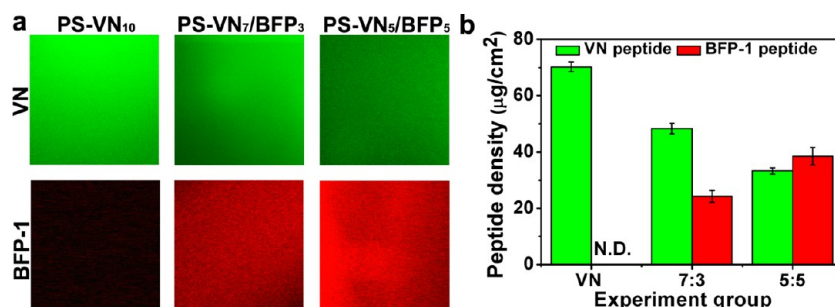


Figure 3. Quantification of peptide content on the mixed-peptides decorated PS surfaces by fluorescent labeling. (a) Visualization of fluorescently labeled peptides (FITC-VN peptide and Rhodamine-BFP-1 peptide) immobilized onto PS substrates. (b) Quantitative peptide intensity of the peptides-decorated substrates with different volume ratios ($n = 6$).

BFP₅ was used as a representative of peptides-conjugated PS substrates (PS-peptide). As depicted in Figure 2a, the pristine PS dish was relatively hydrophobic with a contact angle of $\sim 65^\circ$, which decreased to an average value of 43° after the coating of pDA and further to about 28° after CMC attachment. This could be due to the hydrophilic groups ($-\text{OH}$, $-\text{COOH}$, and $-\text{NH}_2$) of the grafted polymers on the PS surfaces. After immobilizing peptide onto the CMC-modified surface, the contact angle continuously reduced to $\sim 14^\circ$, attributed to the superhydrophilic property of peptide.

These findings were further verified by an XPS survey scan (Figure 2b, Table S2 and Figure S1, Supporting Information). Carbon and oxygen elements are the predominant components of the pristine PS substrate, while a small amount of nitrogen was also recognizable, attributed to unavoidable contamination. Successful anchoring of pDA was indicated by an increase in the N 1s and O 1s contents and a corresponding decrease in the C 1s content from 72.96% to 63.56% as shown in Table S2, Supporting Information. Meanwhile, the nitrogen-to-carbon (N/C) ratio was about 0.126 on PS-pDA, which was similar to the theoretical N/C of 0.125 for dopamine. However, these changes were further aggravated after the grafting of CMC on

the pDA-treated substrate, indicating the immobilization of CMC. Upon attachment of peptide on the surface, notably in the wide-scan spectrum, the appearance of sodium signal (because the peptide was dissolved in PBS buffer) and the enhancement of nitrogen peaks (N 1s, 14.65%) on the surface of PS-peptide indicated the successful tethering of peptide. Furthermore, an evident change in carbon bond composition observed in the high-resolution narrow carbon spectra (C 1s) clearly supported these conclusions (Figure S1, Supporting Information). The high-resolution C 1s spectrum of the pristine PS was deconvoluted into three different curves. The binding energies centered at 284.7, 286.1, and 291.1 eV could be assigned to the $-\text{C}-\text{C}-/\text{-C}-\text{H}-$, $-\text{C}-\text{OH}$, $-\text{C}(\text{O})\text{O}-$ bonds, respectively. After pDA coating, the intensity of the carbon skeleton ($-\text{C}-\text{C}-/\text{-C}-\text{H}-$) decreased dramatically, and the peaks of the hydroxyl ($-\text{C}-\text{OH}$) and carbonyl ($-\text{C}=\text{O}$) groups increased as shown in Figure S1b, Supporting Information. They should be attributed to the catechol/quinone groups of pDA, whereas a broad peak $-\text{C}-\text{N}-$ bond at about 285.5 eV was newly recorded on both PS-CMC and PS-peptide samples, indicating the presence of CMC and peptide. Compared with those of PS-pDA, the peaks of $-\text{C}=\text{O}$

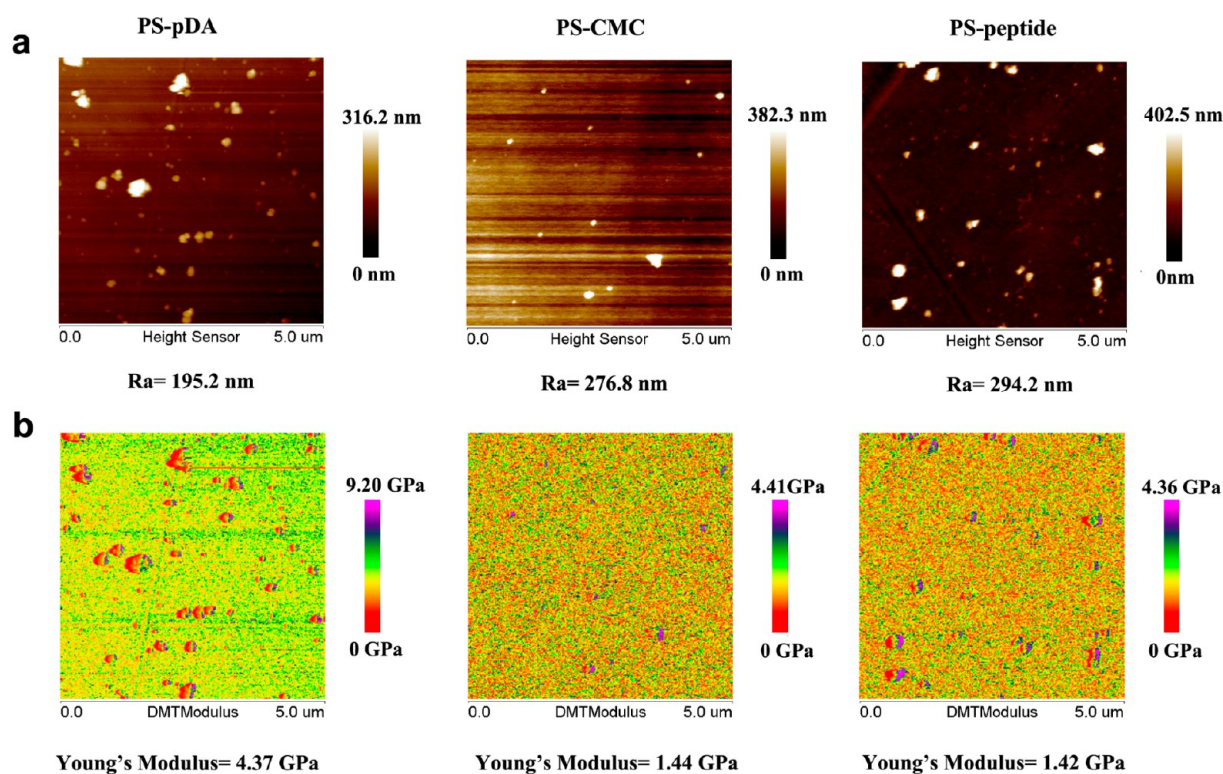


Figure 4. AFM morphology images (a) and property map of the Young's modulus (b) of functionalized PS substrates at different stages: PS-pDA, PS-CMC, and PS-peptide substrates.

O and $-C-N-$ enhanced greatly in intensity due to the abundance of amine groups and amido bonds ($-NH-C=O$) in the structure of peptide molecule, which further proved the successful peptide tethering. These results obviously suggested that peptide was easily immobilized on the CMC-functionalized PS surface assisted by pDA coating.

The peptides have been confirmed to conjugate on the modified PS surfaces from the results mentioned above; afterward, it is important to determine whether they were immobilized at the presupposed volume ratios. As shown in Figure 3a, the uniform fluorescence distribution was observed in different experiment groups, which signified the homogeneity of peptides on the surfaces. No red light was detected on pure VN peptide-treated PS surface. Furthermore, the intensity of green light (VN) gradually decreased and red light (BFP-1) gradually increased on the different peptide ratios treated samples, implying that the VN and BFP-1 peptide were successfully immobilized at the designed ratios. The trend of fluorescence intensity changes was further confirmed by the quantification results in Figure 3b. On the basis of the calculations, VN concentrations in PS-VN₁₀ and PS-VN₅/BFP₅ yielded 70.24 ± 1.73 and $33.28 \pm 1.11 \mu\text{g}/\text{cm}^2$ peptide density, respectively. When reacted with VN/BFP-1 = 5:5 solution, approximately $38.50 \pm 3.04 \mu\text{g}/\text{cm}^2$ BFP-1 was immobilized on the PS-VN₅/BFP₅ plates, and almost no BFP-1 was detected in PS-VN₁₀.

The surface roughness, morphology, and mechanical property of PS substrate were altered by pDA coating or pDA-mediated CMC and peptide immobilization. SEM images showed that bare PS dish had a smooth surface morphology compared with modified PS substrates (Figure 2c). The polymerized DA particles were observed on the surface of pDA-coated PS sample. There were some wrinkles combined

with pDA particles on the PS-CMC surface because CMC tended to form a macromolecule membrane on the surface. However, the addition of a small molecule peptide slightly increased the surface morphology/roughness of PS-CMC substrates. AFM results (Figure 4a) affirmed the SEM analysis, where partial aggregates of polymerized dopamine were found on all pDA-treated surfaces, which confirmed the presence of pDA layer. The pDA aggregates could be easily detected compared to CMC and peptide due to their greater roughness. The average roughness (R_a) value of the decorated PS surfaces, as measured from AFM, indicated that the coating of the CMC biomacromolecule and peptide enhanced the surface roughness of PS substrate. To evaluate the influence of pDA coating and pDA-mediated biopolymers (CMC and peptide) on the mechanical properties of PS substrate, their Young's modulus was measured at the nanoscale using a recently developed AFM surface property mapping technique: PeakForce QNM AFM. PeakForce tapping provides high-resolution mapping of the nanomechanical properties for each sample and exerts a maximum force control of the sample while eliminating lateral forces. In addition, the maximum force exerted on the sample is maintained constant, which is beneficial for delicate biological samples.^{40,41} Using the DMT model as the analysis software, the absolute modulus of each sample could be acquired by calibration of the tip radius and spring constant. In order to have reliable results for the Young's modulus, the deformation value was kept in the range of 1–2 nm for all measurements. It could be seen in Table S3, Supporting Information, that the required peak force set point for deforming the pDA-coated PS was much higher than needed for achieving a similar deformation of the CMC layers, reflecting that the CMC coating was significantly softer than the pDA layer. From the property map of the Young's modulus and quantitative data in

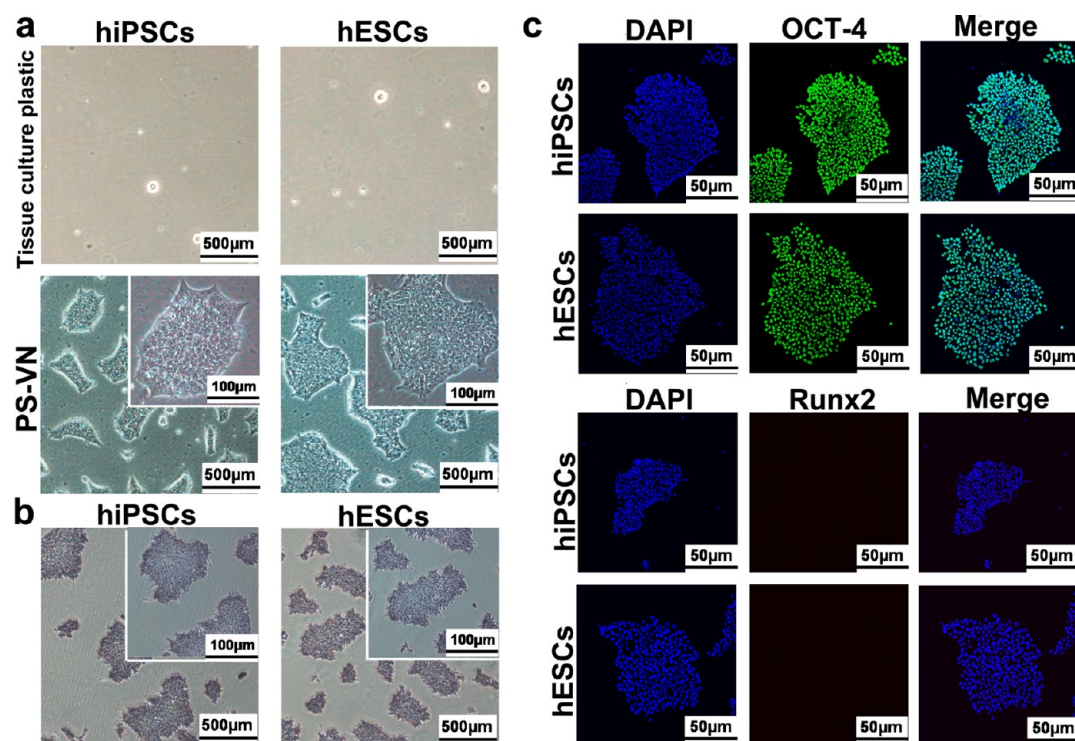


Figure 5. Cell adhesion and pluripotency of the undifferentiated hPSCs cultured on the VN peptide-decorated substrates at day 0. (a) Microscopic images. (b) Alkaline phosphatase staining. (c) Immunofluorescence staining for OCT-4 (green) and Runx2 (red) visualized by laser confocal microscopy. Nuclei were stained blue with DAPI.

Figure 4b, the partial pDA aggregates displayed higher modulus, and the average modulus of the pDA-coated PS substrate was about 4.37 GPa, which was in good agreement with a previous result acquired by AFM-based microtensile testing. Compared with PS-pDA, PS-CMC (1.44 GPa) displayed a lower modulus (about one-third value of that in PS-pDA) with a more uniform mechanical distribution, because CMC polysaccharide was a soft biopolymer having a low biomechanical property. However, peptide immobilization onto the PS-CMC did not reduce the Young's modulus significantly (1.42 GPa), suggesting that short peptide had little influence on the surface mechanical property of CMC-grafted PS plate. These results indicated that modification of the biomacromolecule could alter the biomechanical property of the PS substrate and endow the stiff PS substrate with a soft surface.

As is well known, ECM is a complex mixture of structural proteins (collagen, vitronectin, and fibronectin), polysaccharides (glycosaminoglycans), and signaling proteins such as growth factors.⁴² Together, the components of the ECM offer physical and biochemical cues for cells to attach, grow, proliferate, migrate, and differentiate.⁴³ In this hPSCs culture microenvironment, VN peptide containing the RGD (Arg-Gly-Asp) sequence, as a common cell adhesion motif, plays a pivotal role in attachment of hPSCs. The structure of CMC is similar to glycosaminoglycans, and it has been reported that CMC can promote the expression of ECM in human osteoblasts and chondrocytes and stimulate the differentiation of osteoprogenitor cells.⁴⁴ On the other hand, CMC polysaccharide possesses a low biomechanical attribute close to that of ECM, and it is proof that a soft surface is beneficial to hPSCs culture.⁴⁵ Moreover, BFP-1 peptide enables mimicking the function of BMP-7 protein in the osteogenic niche of bone tissue²⁹ and possibly provides a large drive to osteogenic

differentiation of hPSCs. Thus, our developed peptides-decorated osteogenic niche that mimics some important features of the ECM in terms of hPSCs growth, organization, and differentiation could offer a favorable microenvironment (chemical and physical cues) for culture and osteo-differentiation of hPSCs and demonstrates great potential in bone regenerative medicine.

3.2. Cell Adhesion, Proliferation, and Pluripotency on VN Peptide-Decorated Microenvironment. Assisted by facile pDA technology, a chemically defined and well-controlled 2D cell microenvironment has been established for hPSCs propagation and osteogenic differentiation; next, we are eager to know whether the peptides-decorated niche could support the pluripotency and proliferation of hPSCs in vitro. The pluripotency of hPSCs on pure VN peptide-conjugated PS surface was confirmed by morphology observation and immunofluorescent staining. As shown in Figures S2, Supporting Information, and 5a, there were no hPSCs on the pure CMC substrate and bare tissue culture plastic (negative control) without conjugation of peptides, indicating hPSCs could not attach and grow on these surfaces. However, the newly planted colonies with a uniform distribution were able to attach robustly 1 day after single cells seeding and showed significant spreading on VN peptide-decorated substrate. The cells maintained a typical undifferentiated morphology on the substrate, as characterized by compact colonies with defined edges and large nuclei-to-cytoplasm ratios (Figure 5a), and they stained strongly positive for ALP (Figure 5b) and OCT-4 (Figure 5c), which are typical markers for an undifferentiated state of hPSCs,^{3,46} whereas the cell aggregates were negative for Runx2 (Figure 5c) (a characteristic indicator of osteogenic differentiation of cells), indicating that the aggregates did not contain any osteogenic progenitors.⁴⁷ VN peptide is one

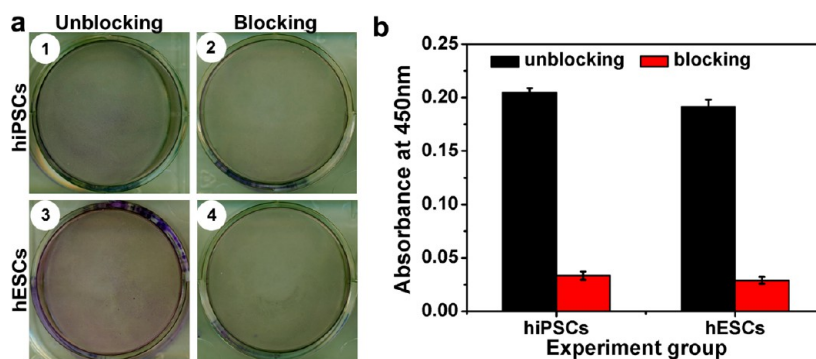


Figure 6. Role of integrin $\alpha_v\beta_3$ receptor in hPSCs adhesion to pDA-VN surfaces. (a) Scanning images of cell attachment at 1 h postseeding before/after integrin $\alpha_v\beta_3$ treatment. (b) Cell adhesion of hPSCs evaluated by CCK-8 assay at 1 h postseeding before/after integrin $\alpha_v\beta_3$ treatment.

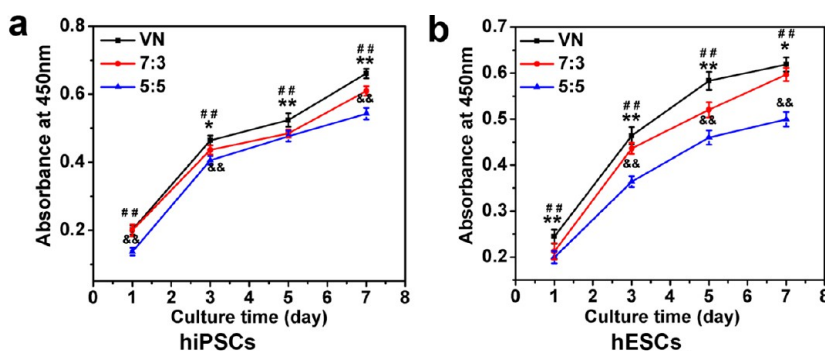


Figure 7. Cell proliferation of hiPSCs (a) and hESCs (b) cultured on the peptides-decorated substrates evaluated by CCK-8 assay at specific time intervals ($n = 3$). *, #, and & represent statistical significance between VN and 7:3 group, VN and 5:5 group, 7:3 and 5:5 group, respectively (*, #, and &, $p < 0.05$; **, ##, and &&, $p < 0.01$).

composition of human ECM, and our previous studies together with other group's research demonstrated that this peptide could support the adhesion and successful propagation of hPSCs for >15 passages via RGD-cell integrin ($\alpha_v\beta_3$ receptor) interaction.^{22,28} With the purpose of providing direct evidence of the specific interaction between cell adhesion and RGD, the integrin-blocking assay was carried out. As shown in Figure 6, after treating hPSCs with the integrin $\alpha_v\beta_3$ antibodies, an obvious decline (up to 86%) of the cell numbers was observed, demonstrating that engagement of $\alpha_v\beta_3$ receptor was sufficient to mediate the cell–ECM interaction in hPSCs grown on the surfaces decorated with synthetic RGD-containing peptide from VN. Thus, these results suggested that the grafted VN peptide retained its biological function after being immobilized onto the surface of PS-CMC through pDA coating, and the hESCs/hiPSCs on the VN peptide-conjugated surface maintained pluripotency before osteogenic induction.

Previous literature in the field suggested that the density of VN peptide on the plate surface also played a vital role in the attachment and proliferation of hPSCs.^{22,27} In order to examine the influence of the introduction of BFP-1 peptide into VN peptide-decorated surface on the cell propagation, growth evaluation of hPSCs was conducted via CCK-8 assay for 1 week. Figures 7 and S3 and S4, Supporting Information, showed that all matrices supported the attachment of hPSCs within 7 days of culture, and both hiPSCs and hESCs displayed compact colonies morphology on the different substrate. The OD_{450} value increased with the extension of time, indicating that mixed peptides-decorated surfaces could facilitate the normal proliferation of hPSCs. There was a correlation between VN/BFP-1 ratio (i.e., conjugated VN peptide density) and

hPSCs numbers after 7 days culturing on the mixed peptides-decorated substrates. The cell numbers were enhanced with increasing VN peptide ratios on the CMC-grafted PS substrate from 50% to 100% because more VN peptide contributed to greater amount sites for cell anchor, coinciding with earlier studies.^{22,27} However, for hiPSCs, the viability of cells on the mixed peptides-decorated surfaces (PS-VN₇/BFP₃ and PS-VN₅/BFP₅) displayed little statistical difference from the pure VN peptide-conjugated surface (PS-VN₁₀) from day 1 to day 5, showing similar proliferation in short-term days. With regard to hESCs, similar growth values were detected on days 1, 3, and 7 for PS-VN₇/BFP₃. At day 7, the numbers of hiPSCs/hESCs attached on the PS-VN₇/BFP₃ surface were about 92.23% and 96.42% of that on PS-VN₁₀ surface, respectively, and their amounts on the PS-VN₅/BFP₅ surface were approximate 82.12% and 77.85% of that on PS-VN₁₀ surface, respectively. By 8 days of culture, hPSCs on all matrices grew to reach confluence. In spite of the decreased cell amounts (10%–22%) in VN/BFP-1 combined peptides-decorated surfaces, these prepared substrates had no negative impact on hPSCs growth and proliferation and they still could provide abundant cells for osteogenesis. Following verification that all matrices under investigation supported the attachment and proliferation of hPSCs, the osteogenic differentiation of hPSCs on various peptides-decorated PS surfaces should be assessed.

3.3. Enhanced Osteogenic Differentiation of hPSCs on Peptides-Decorated Microenvironment. For optimal expansion and differentiation of hPSCs in bone regenerative applications, it is critical to design an osteogenic environment that mimics cell niche and induces ossification of cells using chemically defined materials. To evaluate whether the hiPSCs/

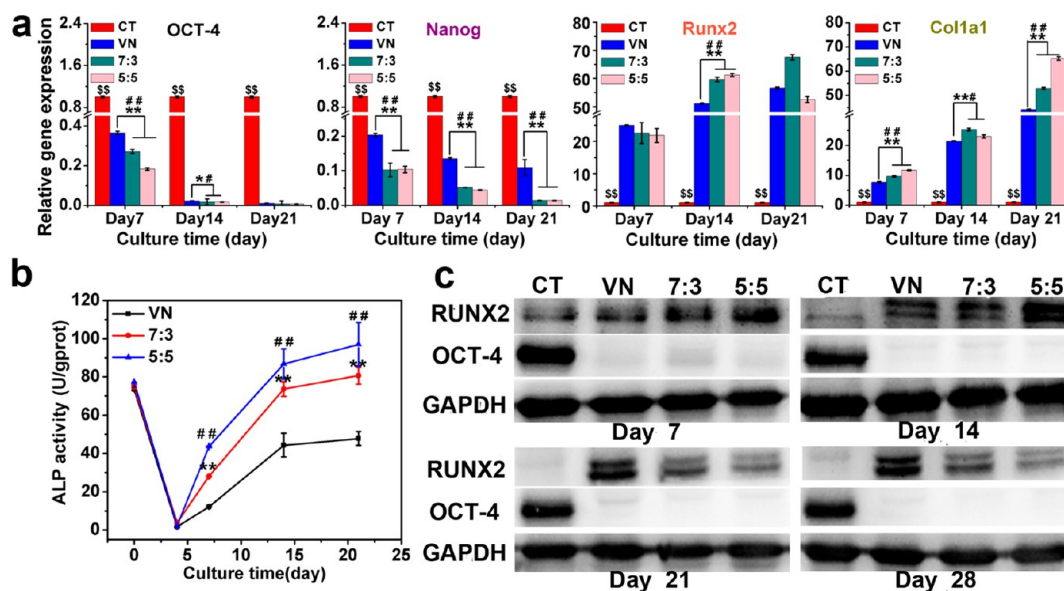


Figure 8. Osteogenic differentiation of hiPSCs cultured on the VN/BFP-1 peptides-decorated PS substrates in vitro at specific time intervals ($n = 3$). CT (i.e., control group) represents the hiPSCs cultured on the bare VN-decorated PS substrate in mTeSR1 medium. \$, *, and # represent statistical significance between CT group and other inducing groups, VN and 7:3 group, VN and 5:5 group, respectively (\$, *, and #, $p < 0.05$; \$\$, **, and ##, $p < 0.01$). (a) qPCR analysis: Gene expressions of OCT-4, Nanog, Runx2 and Col1a1. (b) ALP activity quantification assay. (c) Western blotting analysis: Protein expressions of OCT-4 and Runx2.

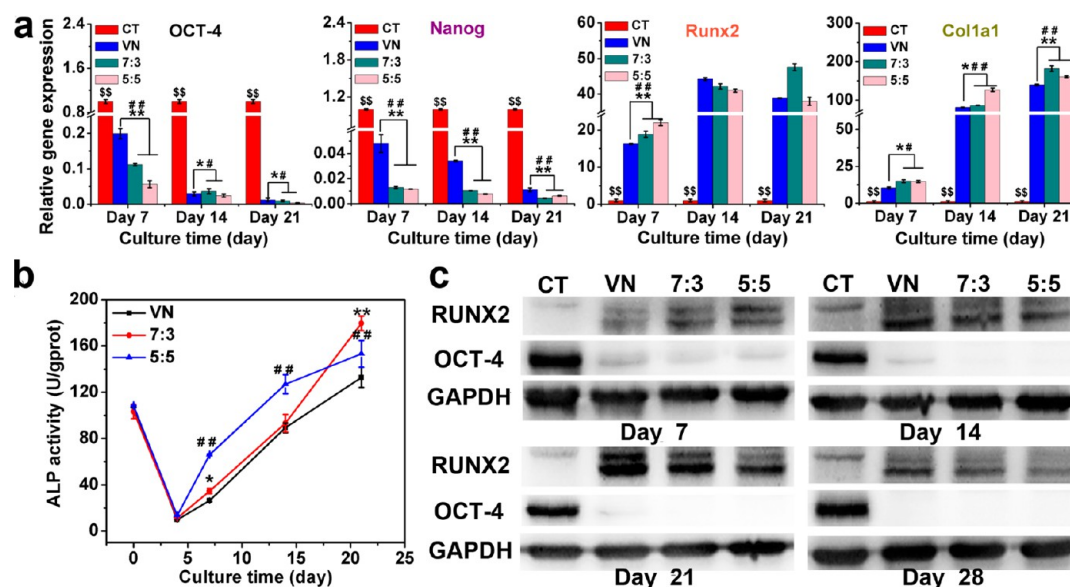


Figure 9. Osteogenic differentiation of hESCs cultured on the VN/BFP-1 peptides-decorated PS substrates in vitro at specific time intervals ($n = 3$). CT (i.e., control group) represents the hESCs cultured on the bare VN-decorated PS substrate in mTeSR1 medium. \$, *, and # represent statistical significance between CT group and other inducing groups, VN and 7:3 group, VN and 5:5 group, respectively (\$, *, and #, $p < 0.05$; \$\$, **, and ##, $p < 0.01$). (a) qPCR analysis: Gene expressions of OCT-4, Nanog, Runx2 and Col1a1. (b) ALP activity quantification assay. (c) Western blotting analysis: Protein expressions of OCT-4 and Runx2.

hESCs enable being directly induced toward osteogenic lineages in vitro, the ALP activity, gene expression, and corresponding protein expression as well as calcium deposition amount were evaluated as previously reported at specific time intervals (days 0, 7, 14, 21, and 28).^{48–51}

3.3.1. Quantification Analysis of Alkaline Phosphate Activity (ALP). ALP, an early marker of osteogenesis, was expressed strongly in the osteoblasts, as well as in undifferentiated hPSCs.⁵² As shown in Figures 8b and 9b, the hPSCs initially displayed a high level of ALP signal and then the signal decreased to a relatively low level after being induced for

4 days, indicating that the hPSCs began to lose their stem cell properties. Later, the expression of ALP began to increase at a relatively stable rate with the extent of time and kept at a high level after 15 days. The re-expression of ALP signal perhaps signified the appearance of osteogenic progenitors after 15 days of osteoinductive culture.³ For hiPSCs (Figure 8b), the ALP signal of BFP-1 peptide-supplied groups reached a significantly higher level than that of pure VN group after 7 days. The ALP level of the PS-VN₇/BFP₃ group and the PS-VN₅/BFP₅ group was 1.69-fold and 2 times that of PS-VN₁₀ group at 21 days, respectively. As for hESCs (Figure 9b), the production of ALP

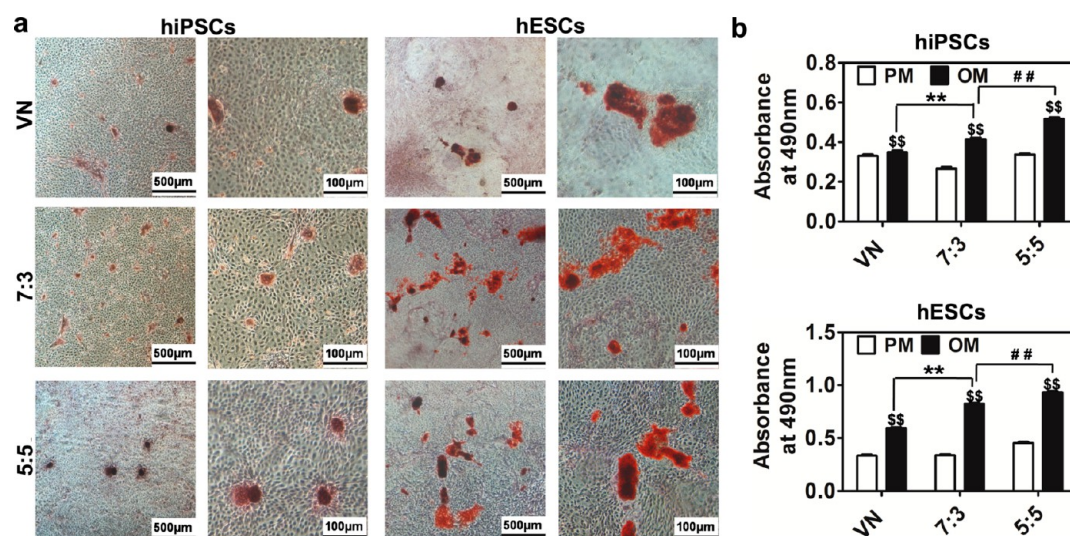


Figure 10. Bone matrix mineralization of hPSCs cultured on the VN/BFP-1 peptides-decorated PS substrates after inducing for 28 days in vitro. (a) ARS staining with lower (scale bar 500 μm) and higher (scale bar 100 μm) magnification. (b) Quantification of ARS staining ($n = 3$). PM and OM separately refer to the hPSCs cultured in the mTeSR1 medium and the osteogenic induction medium. \$, *, and # represent statistical significance between CT group and other inducing groups, VN and 7:3 group, 7:3 and 5:5 group, respectively (\$, *, and #, $p < 0.05$; \$\$, **, and ##, $p < 0.01$).

in the PS-VN₅/BFP₅ group was higher compared with that of the pure VN group from day 7 to day 21. Distinguished with the hiPSCs, at 21 days, the level of ALP expression in the PS-VN₇/BFP₃ group was 1.35 times than that of PS-VN₁₀ sample. In spite of a little different result, the similarity between two hPSCs (i.e., hESCs and hiPSCs) in promoted ALP activity was observed on the BFP-1 peptide-decorated surfaces, implying that the BFP-1 peptide might have an impact on the osteogenesis of hPSCs.

3.3.2. Quantitative Real-Time PCR (qPCR) and Western Blotting Analysis. To understand the action of BFP-1 peptide on hPSCs at the molecular level, the variation of specific genes and proteins expression involved in pluripotency and osteogenesis was examined at different time points as shown in Figures 8 and 9. The hPSCs cultured on the bare VN-decorated PS substrate in mTeSR1 medium (CT, control group) showed nearly unaltered marker gene expression at all time points with high expression of OCT-4 and Nanog makers and no expression of osteogenic makers, indicating the maintenance of pluripotency, whereas qPCR analysis revealed that the pluripotency-associated genes (OCT-4, Nanog) were down-regulated and the osteogenesis-related genes (Runx2, Col1a1) were up-regulated in all groups subjected to osteogenic inducing medium ($p < 0.01$), and their values were a function of culture time. For both cell lines, after being cultured in osteogenic-inducing medium, the expression level of OCT-4 and Nanog began to decrease sharply with time increasing and was kept at an extremely low level near zero after 14 days, which implied that the pluripotency of hPSCs gradually reduced and was totally lost after 14 days. Moreover, for the groups containing of BFP-1 peptide, the pluripotent gene expression was lower than that of pure VN group ($p < 0.05$). Runx2 is the early and master transcription factor, and it regulates the transcription of various osteogenesis-related genes (such as Col1a1, OCN) via binding to the core site of their enhancers or promoters.^{53–55} Col1a1 gene is an osteo-special marker expressed during the later period and encodes the pro-alpha 1 chains of type 1 collagen, which is an extracellular matrix and structural protein contained in the bone matrix.^{56,57}

As found in Figures 8a/9a, the expression peak of Runx2 was the focus on day 14 and that of Col1a1 located on day 21. The reasonable explanation might be that the Runx2 gene is the early marker and triggers the expression of Col1a1. At 14 and 7 days, the Runx2 gene expression level of the PS-VN₇/BFP₃ and PS-VN₅/BFP₅ groups was higher than the PS-VN₁₀ group for hiPSCs and hESCs, respectively. The Runx2 expression of BFP-1 peptide-modified groups began to decrease after 14 days, possibly because the early marker Runx2 functionalized at the prior period and began to degrade after completing its role. In addition, the elevated Col1a1 levels of PS-VN₅/BFP₅ and PS-VN₇/BFP₃ groups were detected compared to the PS-VN₁₀ group for both cell lines from day 7 to day 21. To further verify the results from ALP and qPCR, the dynamics of OCT-4 and Runx2 protein expression was probed. Western blotting analysis (Figures 8c/9c) showed that the expression of OCT-4 protein in inducing groups was lower than that of the control group, and this protein could not be detected after 14 days, corresponding to the findings from qPCR. These results suggested that the cells had lost their pluripotency under the influence of inducing factors and BFP-1 peptide. The expression level of Runx2 protein increased in BFP-1 peptide-decorated groups before 14 days for hiPSCs and before 7 days for hESCs than VN peptide-decorated ones. Afterward, the expression of Runx2 protein in BFP-1 peptide-decorated groups was lower than pure VN group after 14 days. The same dynamic trend was observed in hiPSCs and hESCs. A high expression of Runx2, ALP, and Col1a1 has been reported in the literature;^{29,58} however, the dynamic changes at various stages of the whole osteogenic process have hardly been investigated. BFP-1 peptide derived from the immature region of BMP-7 protein holds the similar osteogenic inducing property and may bind to the same functional sites (BMP receptors), triggering the up-regulation of target osteogenic genes through Smads or mitogen-activated protein kinase (MAPK).^{55,59} These data suggested that the BFP-1 peptide might contribute to the osteogenic potential of the hPSCs.

3.3.3. Alizarin Red S Staining and Quantification Analysis. It is well known that Alizarin Red S could stain extracellular

calcium deposition in bone mineral, which is a special indicator of osteogenic differentiation.^{3,48,60} As seen in Figure 10a, the hPSCs cultured on the VN peptide-decorated surface formed small numbers of bone nodules in osteogenic inducing medium. After combination with the BFP-1 peptide, however, the osteogenic efficiency was greatly enhanced, which was reflected by the greater amounts and larger size of bone nodules compared with the pure PS-VN₁₀ groups. Therefore, BFP-1 peptide might exert a synergistic effect in promoting osteogenesis combined with the traditional osteogenic factors (β -GP, AA, and Dex). Additionally, more intensively distributed and bigger bone nodules were observed on the VN₅/BFP₅-decorated surface. These results were also supported by quantification of the calcium deposition area (Figure 10b). Compared with hPSCs, hMSCs (positive control) generated a large amount of calcium nodules when treated with BMP-7 in osteogenic medium (Figure S5, Supporting Information). On the basis of earlier literature,²⁹ it is effortless for hMSCs to be down an osteogenic path under stimulation of BMP-7 protein. Nevertheless, we still clearly observed a number of red mineral deposits in hiPSCs/hESCs when triggered in the presence of BFP-1 peptide-decorated surface in OM medium similar to that in hMSCs group. Results from ALP activity, qPCR, Western blotting, and Alizarin Red staining have suggested that hPSCs could be directly induced toward osteogenic lineage in the peptides-decorated microenvironment, and the osteogenic efficiency of hPSCs could be further improved by immobilized BFP-1 peptide on the substrate. In future work it is one of our goals to raise the osteogenic differentiation activity of hPSCs in our synthetic peptide-decorated substrate through grafting other chemically defined osteo-differentiation promoting materials on the surface. Several previous reports have shown that nanofibrous scaffold (e.g., poly(L-lactic acid) (PLLA) and poly(ether sulfone) (PES))^{61,62} provide help to enhance the osteogenic differentiation of hPSCs through embryoid bodies (EBs) formation. EBs are commonly used to mimic the three dimensionality of development during gastrulation and formation of the three germ layers in vivo.⁶³ Nevertheless, the limitation of employing EBs for differentiation studies arises from the fact that the yield of desired cells is much lower than the initial amounts of cells.⁶⁴ Currently, without EBs formation step, biomaterialized poly(ethylene glycol)-diacrylate-co-acryloyl-6-aminocaproic acid (PEGDA-co-A6ACA) matrices⁶⁵ and osteomimetic poly(lactic-coglycolic acid) (PLGA) scaffolds⁶⁶ were developed to direct osteogenic differentiation of hESCs. However, these developments required the materials to be coated with Matrigel and ECM protein to promote initial attachment of the hPSCs to the matrix. In the present work, hPSCs might be directly potentiated to osteogenic commitment on our peptides-decorated surface without EBs process and Matrigel/ECM coating (i.e., under chemically defined conditions), which could provide an efficient and safe microenvironment for bone tissue engineering.

4. CONCLUSION

In summary, a chemically defined and safe peptides-decorated 2D culture microenvironment has been developed via pDA chemistry to enhance culture and directed osteogenic differentiation of hPSCs in vitro, which is a simple, time-saving, and efficient method. The ALP activity evaluation, qPCR, and Western blotting combined with ARS results suggested that hPSCs could be induced to osteogenic lineage on the peptides-decorated surface under chemically defined conditions. To the

best of our knowledge, this is the first demonstration of directed osteogenic differentiation of hPSCs by peptides-decorated surface under fully defined conditions. Future work includes the transplantation of hPSCs with peptides-decorated matrices in vivo to study bone tissue formation. This synthetic defined system that supports the process of hPSCs culture to osteo-differentiation has the advantage of eliminating the risks of microbial and viral contamination picked up from mouse feeder cells and animal or human-derived proteins, holding promising potential for bone regenerative medicine.

■ ASSOCIATED CONTENT

Supporting Information

High-resolution spectra of carbon peaks for the pristine and decorated PS substrates; hiPSCs and hESCs morphology on the pure CMC substrate at day 0; hiPSCs and hESCs morphology of different peptides-decorated surfaces from day 1 to day 7; bone matrix mineralization of hMSCs treated with BMP-7 after inducing for 28 days in vitro; primer sequence (5'-3') for the quantitative real-time PCR; elemental composition of the pristine and decorated PS substrates determined by XPS analysis; summary of surface properties of the decorated PS plates determined by means of AFM peak force QNM tapping in air. This material is available free of charge via the Internet at <http://pubs.acs.org>.

■ AUTHOR INFORMATION

Corresponding Authors

*Phone/Fax: +86 10 82195780. E-mail: sc-wei@pku.edu.cn.

*Phone/Fax: +86 10 82196271. E-mail: tang_zhahui@live.cn.

Author Contributions

The manuscript was written through contributions of all authors. All authors have given approval to the final version of the manuscript. M.W. and Y.D. contributed equally.

Notes

The authors declare no competing financial interest.

■ ACKNOWLEDGMENTS

This work was funded by the National Natural Science Foundation of China (No. 81371697), the Key Laboratory of Regenerative Biology, Guangzhou Institutes of Biomedicine and Health, Chinese Academy of Sciences (KLRB201301), and Peking University's 985 Grant. The authors to thank Dr. Longwei Lv for providing the technical assistance.

■ REFERENCES

- (1) Yuan, H.; Fernandes, H.; Habibovic, P.; de Boer, J.; Barradas, A. M.; de Ruiter, A.; Walsh, W. R.; van Blitterswijk, C. A.; de Bruijn, J. D. Osteoinductive Ceramics as a Synthetic Alternative to Autologous Bone Grafting. *Proc. Natl. Acad. Sci. U.S.A.* **2010**, *107*, 13614–13619.
- (2) Wang, H.; Xu, M.; Wu, Z.; Zhang, W.; Ji, J.; Chu, P. K. Biodegradable Poly (Butylene Succinate) Modified by Gas Plasmas and Their In Vitro Functions as Bone Implants. *ACS Appl. Mater. Interfaces* **2012**, *4*, 4380–4386.
- (3) Karp, J. M.; Ferreira, L. S.; Khademhosseini, A.; Kwon, A. H.; Yeh, J.; Langer, R. S. Cultivation of Human Embryonic Stem Cells without the Embryoid Body Step Enhances Osteogenesis In Vitro. *Stem Cells* **2006**, *24*, 835–843.
- (4) Ko, E.; Yang, K.; Shin, J.; Cho, S. W. Polydopamine-Assisted Osteoinductive Peptide Immobilization of Polymer Scaffolds for Enhanced Bone Regeneration by Human Adipose-Derived Stem Cells. *Biomacromolecules* **2013**, *14*, 3202–3213.
- (5) Rhee, S. C.; Ji, Y. H.; Gharibjanian, N. A.; Dhong, E. S.; Park, S. H.; Yoon, E. S. In Vivo Evaluation of Mixtures of Uncultured Freshly

Isolated Adipose-Derived Stem Cells and Demineralized Bone Matrix for Bone Regeneration in a Rat Critically Sized Calvarial Defect Model. *Stem Cells Dev.* **2011**, *20*, 233–242.

(6) Heng, B. C.; Cao, T.; Stanton, L. W.; Robson, P.; Olsen, B. Strategies for Directing the Differentiation of Stem Cells into the Osteogenic Lineage In Vitro. *J. Bone Miner. Res.* **2004**, *19*, 1379–1394.

(7) Lu, L. X.; Zhang, X. F.; Wang, Y. Y.; Ortiz, L.; Mao, X.; Jiang, Z. L.; Xiao, Z. D.; Huang, N. P. Effects of Hydroxyapatite-Containing Composite Nanofibers on Osteogenesis of Mesenchymal Stem Cells In Vitro and Bone Regeneration In Vivo. *ACS Appl. Mater. Interfaces* **2013**, *5*, 319–330.

(8) Chien, C. Y.; Tsai, W. B. Poly (Dopamine)-Assisted Immobilization of Arg-Gly-Asp Peptides, Hydroxyapatite, and Bone Morphogenic Protein-2 on Titanium to Improve the Osteogenesis of Bone Marrow Stem Cells. *ACS Appl. Mater. Interfaces* **2013**, *5*, 6975–6983.

(9) Liu, X.; Feng, Q.; Bachhuka, A.; Vasilev, K. Surface Modification by Allylamine Plasma Polymerization Promotes Osteogenic Differentiation of Human Adipose-Derived Stem Cells. *ACS Appl. Mater. Interfaces* **2014**, *6*, 9733–9741.

(10) Grayson, W. L.; Frohlich, M.; Yeager, K.; Bhumiratana, S.; Chan, M. E.; Cannizzaro, C.; Wan, L. Q.; Liu, X. S.; Guo, X. E.; Vunjak-Novakovic, G. Engineering Anatomically Shaped Human Bone Grafts. *Proc. Natl. Acad. Sci. U.S.A.* **2010**, *107*, 3299–3304.

(11) Illich, D. J.; Demir, N.; Stojkovic, M.; Scheer, M.; Rothamel, D.; Neugebauer, J.; Hescheler, J.; Zöllner, J. E. Concise Review: Induced Pluripotent Stem Cells and Lineage Reprogramming: Prospects for Bone Regeneration. *Stem Cells* **2011**, *29*, 555–563.

(12) Raggi, C.; Berardi, A. C. Mesenchymal Stem Cells, Aging and Regenerative Medicine. *Muscles Ligaments Tendons J.* **2012**, *2*, 239–242.

(13) Kassem, M.; Abdallah, B. M. Human Bone-Marrow-Derived Mesenchymal Stem Cells: Biological Characteristics and Potential Role in Therapy of Degenerative Diseases. *Cell Tissue Res.* **2008**, *331*, 157–163.

(14) Amabile, G.; Meissner, A. Induced Pluripotent Stem Cells: Current Progress and Potential for Regenerative Medicine. *Trends Mol. Med.* **2009**, *15*, 59–68.

(15) Brunner, E. W.; Jurewicz, I.; Heister, E.; Fahimi, A.; Bo, C.; Sear, R. P.; Donovan, P. J.; Dalton, A. B. Growth and Proliferation of Human Embryonic Stem Cells on Fully Synthetic Scaffolds Based on Carbon Nanotubes. *ACS Appl. Mater. Interfaces* **2014**, *6*, 2598–2603.

(16) Nelson, T. J.; Martinez-Fernandez, A.; Terzic, A. Induced Pluripotent Stem Cells: Developmental Biology to Regenerative Medicine. *Nat. Rev. Cardiol.* **2010**, *7*, 700–710.

(17) Takahashi, K.; Tanabe, K.; Ohnuki, M.; Narita, M.; Ichisaka, T.; Tomoda, K.; Yamanaka, S. Induction of Pluripotent Stem Cells from Adult Human Fibroblasts by Defined Factors. *Cell* **2007**, *131*, 861–872.

(18) Higuchi, A.; Ling, Q. D.; Kumar, S.; Munusamy, M.; Alarfajj, A. A.; Umezawa, A.; Wu, G. J. Design of Polymeric Materials for Culturing Human Pluripotent Stem Cells: Progress Toward Feeder-Free and Xeno-Free Culturing. *Prog. Polym. Sci.* **2014**, *39*, 1348–1374.

(19) Xu, C.; Inokuma, M. S.; Denham, J.; Golds, K.; Kundu, P.; Gold, J. D.; Carpenter, M. K. Feeder-Free Growth of Undifferentiated Human Embryonic Stem Cells. *Nat. Biotechnol.* **2001**, *19*, 971–974.

(20) Rodin, S.; Domogatskaya, A.; Strom, S.; Hansson, E. M.; Chien, K. R.; Inzunza, J.; Hovatta, O.; Tryggvason, K. Long-Term Self-Renewal of Human Pluripotent Stem Cells on Human Recombinant Laminin-511. *Nat. Biotechnol.* **2010**, *28*, 611–615.

(21) Braam, S. R.; Zeinstra, L.; Litjens, S.; Ward-van, O. D.; van den Brink, S.; van Laake, L.; Lebrin, F.; Kats, P.; Hochstenbach, R.; Passier, R.; Sonnenberg, A.; Mummery, C. L. Recombinant Vitronectin is a Functionally Defined Substrate that Supports Human Embryonic Stem Cell Self-Renewal via Alpha5beta1 Integrin. *Stem Cells* **2008**, *26*, 2257–2265.

(22) Deng, Y.; Zhang, X.; Zhao, X.; Li, Q.; Ye, Z.; Li, Z.; Liu, Y.; Zhou, Y.; Ma, H.; Pan, G.; Pei, D.; Fang, J.; Wei, S. Long-Term Self-Renewal of Human Pluripotent Stem Cells on Peptide-Decorated

Poly(OEGMA-co-HEMA) Brushes under Fully Defined Conditions. *Acta Biomater.* **2013**, *9*, 8840–8850.

(23) Ross, A. M.; Nandivada, H.; Ryan, A. L.; Lahann, J. Synthetic Substrates for Long-Term Stem Cell Culture. *Polymer* **2012**, *53*, 2533–2539.

(24) Klim, J. R.; Li, L.; Wrighton, P. J.; Piekarczyk, M. S.; Kiessling, L. L. A Defined Glycosaminoglycan-Binding Substratum for Human Pluripotent Stem Cells. *Nat. Methods* **2010**, *7*, 989–994.

(25) Kim, M. J.; Lee, B.; Yang, K.; Park, J.; Jeon, S.; Um, S. H.; Kim, D. I.; Im, S. G.; Cho, S. W. BMP-2 Peptide-Functionalized Nanopatterned Substrates for Enhanced Osteogenic Differentiation of Human Mesenchymal Stem Cells. *Biomaterials* **2013**, *34*, 7236–7246.

(26) Panda, J. J.; Dua, R.; Mishra, A.; Mitra, B.; Chauhan, V. S. 3D Cell Growth and Proliferation on a RGD Functionalized Nanofibrillar Hydrogel Based on a Conformationally Restricted Residue Containing Dipeptide. *ACS Appl. Mater. Interfaces* **2010**, *2*, 2839–2848.

(27) Melkounian, Z.; Weber, J. L.; Weber, D. M.; Fadeev, A. G.; Zhou, Y.; Dolley-Sonneville, P.; Yang, J.; Qiu, L.; Priest, C. A.; Shogbon, C.; Martin, A. W.; Nelson, J.; West, P.; Beltzer, J. P.; Pal, S.; Brandenberger, R. Synthetic Peptide-Acrylate Surfaces for Long-Term Self-Renewal and Cardiomyocyte Differentiation of Human Embryonic Stem Cells. *Nat. Biotechnol.* **2010**, *28*, 606–610.

(28) Jin, S.; Yao, H.; Weber, J. L.; Melkounian, Z. K.; Ye, K. A Synthetic, Xeno-Free Peptide Surface for Expansion and Directed Differentiation of Human Induced Pluripotent Stem Cells. *PLoS One* **2012**, *7*, e50880.

(29) Kim, H. K.; Kim, J. H.; Park, D. S.; Park, K. S.; Kang, S. S.; Lee, J. S.; Jeong, M. H.; Yoon, T. R. Osteogenesis Induced by a Bone Forming Peptide from the Prodomain Region of BMP-7. *Biomaterials* **2012**, *33*, 7057–7063.

(30) Lee, Y. J.; Lee, J. H.; Cho, H. J.; Kim, H. K.; Yoon, T. R.; Shin, H. Electrospun Fibers Immobilized with Bone Forming Peptide-1 Derived from BMP7 for Guided Bone Regeneration. *Biomaterials* **2013**, *34*, 5059–5069.

(31) Shi, Z.; Neoh, K. G.; Kang, E. T.; Poh, C. K.; Wang, W. Surface Functionalization of Titanium with Carboxymethyl Chitosan and Immobilized Bone Morphogenetic Protein-2 for Enhanced Osseointegration. *Biomacromolecules* **2009**, *10*, 1603–1611.

(32) Jayakumar, R.; Prabakaran, M.; Nair, S.; Tokura, S.; Tamura, H.; Selvamurugan, N. Novel Carboxymethyl Derivatives of Chitin and Chitosan Materials and Their Biomedical Applications. *Prog. Mater. Sci.* **2010**, *55*, 675–709.

(33) Chen, R. N.; Wang, G. M.; Chen, C. H.; Ho, H. O.; Sheu, M. T. Development of N, O-(Carboxymethyl) Chitosan/Collagen Matrixes as a Wound Dressing. *Biomacromolecules* **2006**, *7*, 1058–1064.

(34) Budiraharjo, R.; Neoh, K. G.; Kang, E. T. Hydroxyapatite-Coated Carboxymethyl Chitosan Scaffolds for Promoting Osteoblast and Stem Cell Differentiation. *J. Colloid Interface Sci.* **2012**, *366*, 224–232.

(35) Mishra, D.; Bhunia, B.; Banerjee, I.; Datta, P.; Dhara, S.; Maiti, T. K. Enzymatically Crosslinked Carboxymethyl-Chitosan/Gelatin/Nano-Hydroxyapatite Injectable Gels for In Situ Bone Tissue Engineering Application. *Mater. Sci. Eng., C: Mater. Biol. Appl.* **2011**, *31*, 1295–1304.

(36) Lee, H.; Dellatore, S. M.; Miller, W. M.; Messersmith, P. B. Mussel-Inspired Surface Chemistry for Multifunctional Coatings. *Science* **2007**, *318*, 426–430.

(37) Cho, H. J.; Perikamana, S. K.; Lee, J. H.; Lee, J.; Lee, K. M.; Shin, C. S.; Shin, H. Effective Immobilization of BMP-2 Mediated by Polydopamine Coating on Biodegradable Nanofibers for Enhanced In Vivo Bone Formation. *ACS Appl. Mater. Interfaces* **2014**, *6*, 11225–11235.

(38) Lyngø, M. E.; van der Westen, R.; Postma, A.; Stadler, B. Polydopamine-a Nature-Inspired Polymer Coating for Biomedical Science. *Nanoscale* **2011**, *3*, 4916–4928.

(39) Yang, K.; Lee, J. S.; Kim, J.; Lee, Y. B.; Shin, H.; Um, S. H.; Kim, J. B.; Park, K. I.; Lee, H.; Cho, S. W. Polydopamine-Mediated Surface

Modification of Scaffold Materials for Human Neural Stem Cell Engineering. *Biomaterials* **2012**, *33*, 6952–6964.

(40) Liu, Y.; Luo, D.; Kou, X. X.; Wang, X. D.; Tay, F. R.; Sha, Y. L.; Gan, Y. H.; Zhou, Y. H. Hierarchical Intrafibrillar Nanocarbonated Apatite Assembly Improves the Nanomechanics and Cytocompatibility of Mineralized Collagen. *Adv. Funct. Mater.* **2013**, *23*, 1404–1411.

(41) Sweers, K.; van der Werf, K.; Bennink, M.; Subramaniam, V. Nanomechanical Properties of Alpha-Synuclein Amyloid Fibrils: a Comparative Study by Nanoindentation, Harmonic Force Microscopy, and Peakforce QNM. *Nanoscale Res. Lett.* **2011**, *6*, 270.

(42) Frantz, C.; Stewart, K. M.; Weaver, V. M. The Extracellular Matrix at a Glance. *J. Cell Sci.* **2010**, *123*, 4195–4200.

(43) Hernandez-Gordillo, V.; Chmielewski, J. Mimicking the Extracellular Matrix with Functionalized, Metal-Assembled Collagen Peptide Scaffolds. *Biomaterials* **2014**, *35*, 7363–7373.

(44) Lahiji, A.; Sohrabi, A.; Hungerford, D. S.; Frondoza, C. G. Chitosan Supports the Expression of Extracellular Matrix Proteins in Human Osteoblasts and Chondrocytes. *J. Biomed. Mater. Res.* **2000**, *51*, 586–595.

(45) Chowdhury, F.; Li, Y.; Poh, Y. C.; Yokohama-Tamaki, T.; Wang, N.; Tanaka, T. S. Soft Substrates Promote Homogeneous Self-Renewal of Embryonic Stem Cells via Downregulating Cell-Matrix Traction. *PLoS One* **2010**, *5*, e15655.

(46) Chang, C. W.; Hwang, Y.; Brafman, D.; Hagan, T.; Phung, C.; Varghese, S. Engineering Cell-Material Interfaces for Long-Term Expansion of Human Pluripotent Stem Cells. *Biomaterials* **2013**, *34*, 912–921.

(47) Levi, B.; Hyun, J. S.; Montoro, D. T.; Lo, D. D.; Chan, C. K.; Hu, S.; Sun, N.; Lee, M.; Grova, M.; Connolly, A. J.; Wu, J. C.; Gurtner, G. C.; Weissman, I. L.; Wan, D. C.; Longaker, M. T. In Vivo Directed Differentiation of Pluripotent Stem Cells for Skeletal Regeneration. *Proc. Natl. Acad. Sci. U.S.A.* **2012**, *109*, 20379–20384.

(48) Liu, J.; Chen, W.; Zhao, Z.; Xu, H. H. Reprogramming of Mesenchymal Stem Cells Derived from iPSCs Seeded on Biofunctionalized Calcium Phosphate Scaffold for Bone Engineering. *Biomaterials* **2013**, *34*, 7862–7872.

(49) Zou, L.; Luo, Y.; Chen, M.; Wang, G.; Ding, M.; Petersen, C. C.; Kang, R.; Dagnaes-Hansen, F.; Zeng, Y.; Lv, N.; Ma, Q.; Le, D. Q.; Besenbacher, F.; Bolund, L.; Jensen, T. G.; Kjems, J.; Pu, W. T.; Bünger, C. A Simple Method for Deriving Functional MSCs and Applied for Osteogenesis in 3D Scaffolds. *Sci. Rep.* **2013**, *3*, 2243.

(50) de Peppo, G. M.; Marcos-Campos, I.; Kahler, D. J.; Alsalmal, D.; Shang, L.; Vunjak-Novakovic, G.; Marolt, D. Engineering Bone Tissue Substitutes from Human Induced Pluripotent Stem Cells. *Proc. Natl. Acad. Sci. U.S.A.* **2013**, *110*, 8680–8685.

(51) Kang, H.; Shih, Y. R.; Hwang, Y.; Wen, C.; Rao, V.; Seo, T.; Varghese, S. Mineralized Gelatin Methacrylate-Based Matrices Induce Osteogenic Differentiation of Human Induced Pluripotent Stem Cells. *Acta Biomater.* **2014**, *7061*, 00346–8.

(52) Draper, J. S.; Pigott, C.; Thomson, J. A.; Andrews, P. W. Surface Antigens of Human Embryonic Stem Cells: Changes upon Differentiation in Culture*. *J. Anat.* **2002**, *200*, 249–258.

(53) Wu, H.; Whitfield, T. W.; Gordon, J. A.; Dobson, J. R.; Tai, P. W.; van Wijnen, A. J.; Stein, J. L.; Stein, G. S.; Lian, J. B. Genomic Occupancy of Runx2 with Global Expression Profiling Identifies a Novel Dimension to Control of Osteoblastogenesis. *Genome Biol.* **2014**, *15*, R52.

(54) Komori, T. Signaling Networks in RUNX2-Dependent Bone Development. *J. Cell Biochem.* **2011**, *112*, 750–755.

(55) Carreira, A. C.; Lojudice, F. H.; Halcsik, E.; Navarro, R. D.; Sogayar, M. C.; Granjeiro, J. M. Bone Morphogenetic Proteins: Facts, Challenges, and Future Perspectives. *J. Dent. Res.* **2014**, *93*, 335–345.

(56) Kaneto, C. M.; Lima, P. S. P.; Zanette, D. L.; Prata, K. L.; Pina Neto, J. M.; de Paula, F. J.; Silva, W. A., Jr. COL1A1 and MiR-29b Show Lower Expression Levels during Osteoblast Differentiation of Bone Marrow Stromal Cells from Osteogenesis Imperfecta Patients. *BMC Med. Genet.* **2014**, *15*, 45.

(57) Pollitt, R.; McMahon, R.; Nunn, J.; Bamford, R.; Afifi, A.; Bishop, N.; Dalton, A. Mutation Analysis of COL1A1 and COL1A2 in Patients Diagnosed with Osteogenesis Imperfecta Type I-IV. *Hum. Mutat.* **2006**, *27*, 716.

(58) Ko, J. Y.; Kim, K. I.; Park, S.; Im, G. I. In Vitro Chondrogenesis and In Vivo Repair of Osteochondral Defect with Human Induced Pluripotent Stem Cells. *Biomaterials* **2014**, *35*, 3571–3581.

(59) Bandyopadhyay, A.; Yadav, P. S.; Prashar, P. BMP Signaling in Development and Diseases: a Pharmacological Perspective. *Biochem. Pharmacol.* **2013**, *85*, 857–864.

(60) Phillips, M. D.; Kuznetsov, S. A.; Cherman, N.; Park, K.; Chen, K. G.; McClendon, B. N.; Hamilton, R. S.; McKay, R. D.; Chenoweth, J. G.; Mallon, B. S.; Robey, P. G. Directed Differentiation of Human Induced Pluripotent Stem Cells toward Bone and Cartilage: In Vitro versus In Vivo Assays. *Stem Cells Transl. Med.* **2014**, *3*, 867–878.

(61) Ardeshtyrlajimi, A.; Hosseinkhani, S.; Parivar, K.; Yaghmaie, P.; Soleimani, M. Nanofiber-Based Polyethersulfone Scaffold and Efficient Differentiation of Human Induced Pluripotent Stem Cells into Osteoblastic Lineage. *Mol. Biol. Rep.* **2013**, *40*, 4287–4294.

(62) Smith, L. A.; Liu, X.; Hu, J.; Ma, P. X. The Enhancement of Human Embryonic Stem Cell Osteogenic Differentiation with Nano-Fibrous Scaffolding. *Biomaterials* **2010**, *31*, 5526–5535.

(63) Itskovitz-Eldor, J.; Schuldiner, M.; Karsenti, D.; Eden, A.; Yanuka, O.; Amit, M.; Soreq, H.; Benvenisty, N. Differentiation of Human Embryonic Stem Cells into Embryoid Bodies Compromising the Three Embryonic Germ Layers. *Mol. Med.* **2000**, *6*, 88.

(64) Dang, S. M.; Kyba, M.; Perlingeiro, R.; Daley, G. Q.; Zandstra, P. W. Efficiency of Embryoid Body Formation and Hematopoietic Development from Embryonic Stem Cells in Different Culture Systems. *Biotechnol. Bioeng.* **2002**, *78*, 442–453.

(65) Kang, H.; Wen, C.; Hwang, Y.; Shih, Y.-R. V.; Kar, M.; Seo, S. W.; Varghese, S. Biomaterialized Matrix-Assisted Osteogenic Differentiation of Human Embryonic Stem Cells. *J. Mater. Chem. B* **2014**, *2*, 5676–5688.

(66) Rutledge, K. E.; Cheng, Q.; Pryzhkova, M.; Harris, G.; Jabbarzadeh, E. Enhanced Differentiation of Human Embryonic Stem Cells on ECM-Containing Osteomimetic Scaffolds for Bone Tissue Engineering. *Tissue Eng., Part C: Methods* **2014**, *20*, 865–874.